

# INTERLAMINAR FRACTURE CHARACTERIZATION OF A CARBON-EPOXY COMPOSITE IN PURE MODE II

R. D. S. G. Campilho<sup>1,a</sup>, M. F. S. F. de Moura<sup>1,b</sup>, A. M. G. Pinto<sup>2,c</sup>,  
D. A. Ramantani<sup>1,d</sup>

<sup>1</sup> FEUP, Faculdade de Engenharia da Universidade do Porto, R. Dr. Roberto Frias, s/n, 4200-465 Porto, Portugal

<sup>2</sup> ISEP, Instituto Superior de Engenharia do Porto, R. Dr. António Bernardino de Almeida, 431, 4200-072 Porto, Portugal

<sup>a</sup>raulcampilho@hotmail.com, <sup>b</sup>mfmoura@fe.up.pt, <sup>c</sup>agp@isep.ipp.pt,  
<sup>d</sup>dimitramantani@hotmail.com

**Keywords:** Cohesive Damage Model, Finite Element Method, Fracture Characterization, End-Notched Flexure.

**Abstract.** The interlaminar fracture toughness in pure mode II ( $G_{IIc}$ ) of a Carbon-Fibre Reinforced Plastic (CFRP) composite is characterized experimentally and numerically in this work, using the End-Notched Flexure (ENF) fracture characterization test. The value of  $G_{IIc}$  was extracted by a new data reduction scheme avoiding the crack length measurement, named Compliance-Based Beam Method (CBBM). This method eliminates the crack measurement errors, which can be non-negligible, and reflect on the accuracy of the fracture energy calculations. Moreover, it accounts for the Fracture Process Zone (FPZ) effects. A numerical study using the Finite Element Method (FEM) and a triangular cohesive damage model, implemented within interface finite elements and based on the indirect use of Fracture Mechanics, was performed to evaluate the suitability of the CBBM to obtain  $G_{IIc}$ . This was performed comparing the values of  $G_{IIc}$  inputted in the numerical models with the ones resulting from the application of the CBBM to the numerical load-displacement ( $P$ - $\delta$ ) curve. In this numerical study, the Compliance Calibration Method (CCM) was also used to extract  $G_{IIc}$ , for comparison purposes.

## Introduction

Advanced composite materials such as CFRP have recently come to the fore owing to a set of interesting characteristics over the conventional engineering materials such as aluminium or steel. In fact, these high performance composites are being increasingly used in structures requiring high specific strength and stiffness, such as in the automotive, marine, military, aeronautical and aerospace industries. Unidirectional CFRP composites are also ideal for reinforcement purposes, not changing significantly the structures stiffness, and are corrosion resistant. However, it is known that layered composites are prone to develop internal damage, like matrix cracking and delamination, which can be particularly dangerous for the structural stability, often leading to premature catastrophic failures. The internal damage is not easily detectable, which increases the associated risks. In the majority of real applications, matrix cracking and delamination are associated and constitute a typical damage mechanism of composites, especially when structures are submitted to bending loads [1-2]. Thus, the interlaminar fracture toughness characterization of CFRP composites acquires special relevancy in the context of the strength prediction of CFRP structures, and also to study the strength behaviour of adhesively-bonded joints or repairs, since in many occasions damage in these assemblies grows between composite layers, due to a typically smaller strength than the adhesive layer [3-4].

Fracture characterization under pure mode II is usually accomplished using the ENF fracture characterization test [5]. The main advantages of this experimental test are its simplicity and the

possibility to obtain  $G_{IIc}$  mathematically using the beam theory [6]. However, problems related to unstable crack growth and to crack monitoring during propagation are yet not well solved [7]. Actually, in mode II fracture characterization tests, the crack tends to close due to the applied load, which hinders a clear visualization of its tip, difficulting the crack monitoring during propagation required for the classical data reduction schemes, based on beam theory analysis and compliance calibration. On the other hand, a FPZ ahead of the crack tip exists under mode II loading, which affects the measured fracture energy. Consequently, its influence should be taken into account, which does not occur when a real crack length is used in the selected data reduction scheme. Truss et al. [8] studied the interlaminar and intralaminar fracture toughness of a continuous and an aligned discontinuous carbon fibre/epoxy composite using the Compact Tension and Double Cantilever Beam tests. Extensive fibre bridging was found in both interlaminar and intralaminar tests. The authors concluded that the misalignment in the discontinuous fibre samples increases the fracture toughness at initiation and propagation.

In this work, the value of  $G_{IIc}$  of a CFRP laminate is obtained by a new data reduction scheme not requiring the crack length measurement, the CBBM. This method eliminates the crack measurement errors, which can be non-negligible, and reflect on the accuracy of the fracture energy calculations. Moreover, it accounts for the FPZ effects. A comparative study was also performed to validate the CBBM. This analysis employed the FEM and a triangular cohesive damage model, based on the indirect use of Fracture Mechanics and implemented within interface finite elements, to evaluate the suitability of the CBBM to obtain the value of  $G_{IIc}$ . This was accomplished comparing the values of  $G_{IIc}$  inputted in the numerical models with the values obtained applying the CBBM to the numerical  $P$ - $\delta$  curves. The CCM was also applied to the FEM results, for comparison of the results.

## Experimental work

The geometry and dimensions of the ENF specimens are shown in Fig. 1 (a). The specimens consisted of unidirectional  $0^\circ$  lay-ups of carbon/epoxy prepreg (SEAL<sup>®</sup> Texipreg HS 160 RM) with 24 plies of 0.15 mm of unit thickness, whose ply elastic orthotropic properties are presented in Table 1. The initial crack was made introducing a thin Teflon<sup>®</sup> film (thickness of 25  $\mu$ m) during lay-up. Curing of the laminate was accomplished in a press during one hour at 130°C and 4 bar pressure. Six specimens were tested using an INSTRON 5848 electro-mechanical Microtester equipped with a 2kN load cell, at room temperature and under displacement control (2 mm/min). The  $P$ - $\delta$  curve was registered during the test. Fig. 1 (b) shows the test setup.

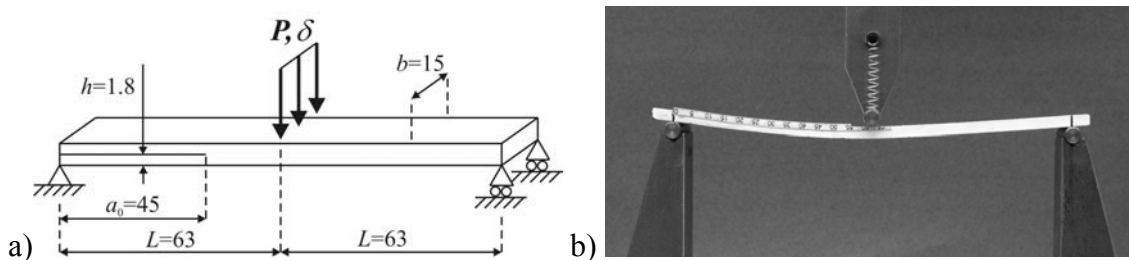


Fig. 1 – ENF specimen geometry (a) and test setup (b).

Table 1 –Elastic orthotropic properties of a unidirectional CFRP ply aligned in direction  $x$  [9].

$E_x=1.09E+05$ MPa	$\nu_{xy}=0.342$	$G_{xy}=4315$ MPa
$E_y=8819$ MPa	$\nu_{xz}=0.342$	$G_{xz}=4315$ MPa
$E_z=8819$ MPa	$\nu_{yz}=0.380$	$G_{yz}=3200$ MPa

## Data reduction schemes

The classical data reduction schemes to obtain  $G_{IIC}$  are usually based on compliance calibration or beam theory. The Compliance Calibration Method (CCM) is based on the Irwin-Kies equation [10]

$$G_{IIC} = \frac{P^2}{2B} \frac{dC}{da}, \quad (1)$$

where  $B$  represents the specimen width,  $a$  the crack length and  $C=\delta/P$  the specimen compliance. Cubic polynomials ( $C=C_1a^3+C_0$ ) were used to fit the  $C=f(a)$  curves, For the CBBM, the compliance equation can be obtained from the Castigliano theorem, using the strain energy of the ENF specimen

$$C = \frac{3a^3 + 2L^3}{12E_x I} + \frac{3L}{10G_{xz} Bh}, \quad (2)$$

with  $I$  being the second moment of inertia of the cracked arm. It should be emphasized that this method constitutes an approach based on beam theory and allows defining the compliance  $C=\delta/P$  of the specimen. However, some issues like stress concentrations at the crack tip and FPZ development, influencing the  $P-\delta$  curve, are not accounted for in the beam theory. To overcome this limitation, a corrected flexural modulus ( $E_f$ ) can be used instead of  $E_x$ . The value of  $E_f$ , individual to each tested specimen, can be obtained from equation (2) using the measured initial compliance ( $C_0$ ) instead of  $C$  and the initial crack length ( $a_0$ ) in place of  $a$

$$E_f = \frac{3a_0^3 + 2L^3}{12I} \left( C_0 - \frac{3L}{10G_{xz} Bh} \right)^{-1}. \quad (3)$$

The effect of the FPZ can be included considering the values of  $C$  and equivalent crack length ( $a_{eq}$ ) during propagation. Combining equations (2) and (3) it can be written

$$a_{eq} = a + \Delta a_{FPZ} = \left[ \frac{C_{corr}}{C_{0corr}} a_0^3 + \frac{2}{3} \left( \frac{C_{corr}}{C_{0corr}} - 1 \right) L^3 \right]^{1/3}, \quad (4)$$

where  $C_{corr}$  is given by

$$C_{corr} = C - \frac{3L}{10G_{13} Bh}. \quad (5)$$

$G_{IIC}$  can now be obtained using the Irwin-Kies equation

$$G_{IIC} = \frac{9P^2 a_{eq}^2}{16B^2 E_f h^3} \quad (6)$$

This method allows the extraction of  $G_{IIC}$  using only the  $P-\delta$  curve. The measurement of the value of  $a$  during propagation is not required because  $a_{eq}$  is used instead of  $a$ . Additionally,  $a_{eq}$  includes the effect of the FPZ, not taken into account when the real crack length is considered.

## Cohesive Damage Model

A mixed-mode (I+II) cohesive damage model was used to simulate damage initiation and propagation. A triangular law between stresses ( $\sigma$ ) and relative displacements ( $\delta_r$ ) between homologous points of the interface finite elements was established (Fig. 2).

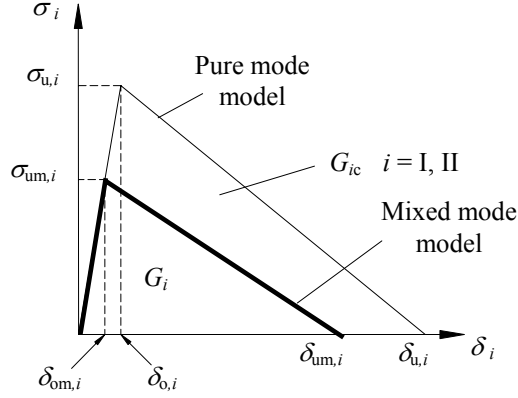


Fig. 2 – Triangular softening law in pure mode and mixed mode.

Damage initiation is predicted using the following quadratic stress criterion

$$\left( \frac{\sigma_I}{\sigma_{u,I}} \right)^2 + \left( \frac{\sigma_{II}}{\sigma_{u,II}} \right)^2 = 1 \quad \text{if } \sigma_I > 0, \quad (7)$$

$$\sigma_{II} = \sigma_{u,II} \quad \text{if } \sigma_I \leq 0$$

where  $\sigma_i$ , ( $i=I, II$ ) corresponds to the stress in a given integration point of an interface element in the respective pure mode. Damage growth is predicted using the linear energetic criterion

$$\frac{G_I}{G_{Ic}} + \frac{G_{II}}{G_{IIc}} = 1. \quad (8)$$

The area under the minor triangle of Fig. 2 represents the energy released in each mode, while the bigger triangle area corresponds to the respective  $G_{Ic}$ . When equation (8) is satisfied, damage propagation occurs and stresses are completely released, with the exception of normal compressive ones. A detailed description of the model can be found in the work of Campilho et al. [11].

## Results

The values of  $G_{IIc}$  were extracted for the six specimens using the CBBM (Table 2). The experimental values of  $G_{IIc}$  showed to be in close agreement, giving an average of  $G_{IIc}=0.84\pm 0.07$  N/mm.

Table 2 – Values of  $G_{IIc}$  obtained by the ENF tests.

<i>Specimen</i>	$G_{IIc}$ [N/mm]	<i>Specimen</i>	$G_{IIc}$ [N/mm]
1	0.80	4	0.86
2	0.89	5	0.85
3	0.94	6	0.73
<i>Avg. <math>G_{IIc}</math></i>		0.84	
<i>St. Dev.</i>		0.07	

Numerical simulations of the ENF tests were performed for each one of the specimens, considering their individual dimensions and values of  $G_{IIc}$ , to verify how the proposed method replicates the inputted value of  $G_{IIc}$ . This will allow an assessment of the CBBM suitability to extract this parameter. The CCM was also considered, for comparison. The numerical  $P$ - $\delta$ - $a$  parameters were collected from the FEM models to obtain the respective  $R$ -curves and estimation of  $G_{IIc}$ . Fig. 3 shows the deformed shape of the ENF specimen during crack propagation, and the respective boundary and loading conditions. The specimen arms were modelled with plane-strain 8-node quadrilateral solid finite elements (CPE8 from ABAQUS<sup>®</sup>). Crack propagation was simulated with 6 node interface finite elements compatible with the ABAQUS<sup>®</sup> elements, including the triangular mixed-mode cohesive damage model presented previously. Each specimen arm was modelled by eight solid finite elements through-thickness. A more refined mesh was considered at the propagation region and near the cylinders. Boundary conditions included fixing the supporting cylinders in the directions  $x$  and  $y$  and restraining the loading cylinder in the direction  $x$ . The lowest node at the specimen mid-section was also restrained in the direction  $x$ .

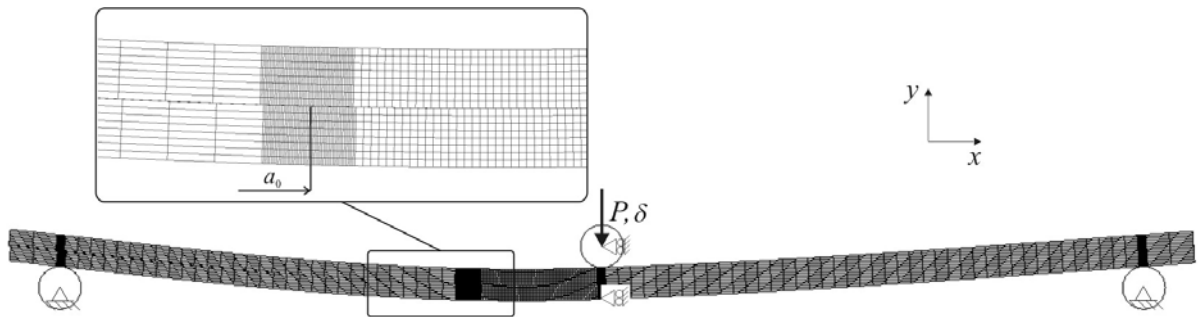


Fig. 3 – ENF specimen during crack propagation, and respective boundary and loading conditions.

Fig. 4 (a) compares the experimental and numerical  $P$ - $\delta$  curves for specimen 3 of Table 2, whilst Fig. 4 (b) relates to the corresponding  $R$ -curves for the same specimen. It was necessary to establish a correspondence between  $a_{eq}$  and  $a$  using the applied displacement, in order to plot the CBBM  $R$ -curve as a function of  $a$ . The good correspondence between the value of  $G_{IIc}$  inputted in the numerical model and the one resulting from the application of the CBBM shows the capabilities of this method for the calculation of  $G_{IIc}$ . A slightly higher deviation was found for the CCM, whose cause will be subsequently discussed.

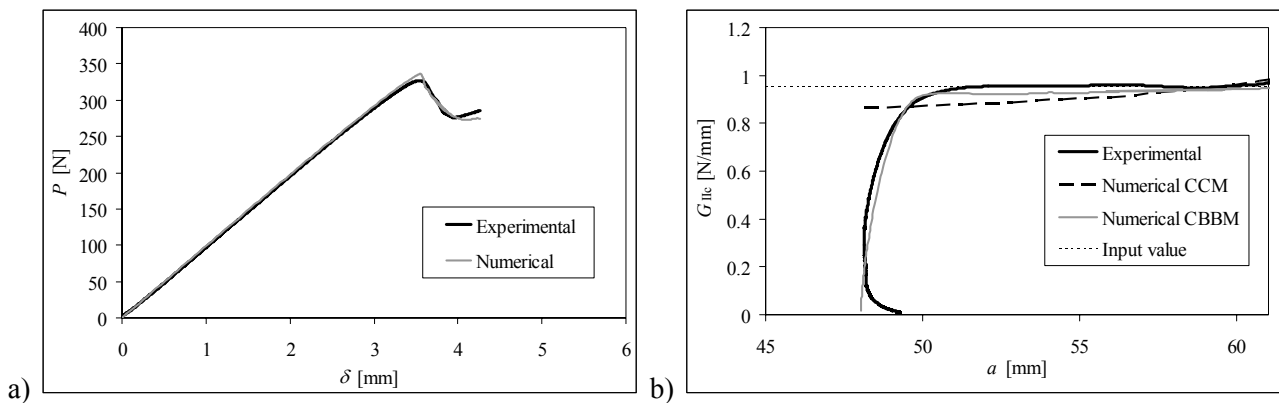


Fig. 4 – Experimental and numerical  $P$ - $\delta$ (a) and  $R$ -curves (b) for specimen 3 (Table 2).

Table 3 shows the results for the six specimens. The average error corresponds to the average of the absolute individual error values. The CBBM estimated accurately the value of  $G_{IIc}$  for all specimens (average error of 1.62%), showing always a slight underprediction, due to spurious mode I during propagation [7]. The CCM showed bigger deviations, explained by polynomial fitting difficulties (average error of 4.54%).

Table 3 – Inputted and predicted  $G_{IIc}$  values [N/mm] using ENF numerical models.

<i>Specimen</i>	<i>Inputted</i>	<i>CCM</i>	<i>Error [%]</i>	<i>CBBM</i>	<i>Error [%]</i>
1	0.80	0.75	-6.25	0.78	-2.50
2	0.89	0.90	1.12	0.87	-2.25
3	0.94	0.88	-6.38	0.93	-1.06
4	0.86	0.90	4.65	0.85	-1.16
5	0.85	0.81	-4.71	0.85	0
6	0.73	0.76	4.11	0.71	-2.74
<i>Average error [%]</i>		4.54		1.62	

### Summary

In this work, a suitable methodology for fracture characterization under pure II was developed. A new data reduction scheme based on the crack equivalent concept was employed to obtain the interlaminar fracture toughness of a carbon-epoxy laminate in pure mode II. The method is advantageous relatively to classical ones as it does not require the crack length measurement during its growth and accounts for the energy dissipated at the Fracture Process Zone. A numerical analysis was also performed to ascertain the suitability of the proposed method for the measurement of the fracture toughness. A triangular mixed-mode cohesive damage model was used to simulate crack initiation and propagation in finite element simulations, allowing the comparison between the inputted values of fracture toughness in pure mode II and the corresponding values extracted by the developed method. The Compliance Calibration Method was also employed in this numerical study, for comparison purposes. This work showed that the proposed method provides accurate results.

### References

1. N. Takeda, R.L. Sierakowski and L.E. Malvern: ASTM STP Vol 4 (1982), p. 40.
2. S.P. Joshi and C.T. Sun: J. Compos. Mater. Vol. 5 (1985), p. 51.
3. R.D.S.G. Campilho, M.F.S.F. de Moura and J.J.M.S. Domingues: Int. J. Solids Struct. Vol. 45 (2008), p. 1497.
4. R.D.S.G. Campilho, M.F.S.F. de Moura, A.M.G. Pinto, J.J.L. Morais and J.J.M.S. Domingues: Compos. Part B Vol. 40 (2009), p. 149.
5. M.F.S.F. de Moura, R.D.S.G. Campilho and J.P.M. Gonçalves: Int. J. Solids Struct. Vol. 46 (2009), p. 1589.
6. H. Yoshihara: Holzforschung Vol. 61 (2007), p. 182.
7. M.F.S.F. de Moura: J. Adhes. Sci. Technol. Vol. 20 (2006), p. 37.
8. R.H. Truss, P.J. Hine and R.A. Duckett: Compos. Part A Vol. 28A (1997), p. 627.
9. R.D.S.G. Campilho, M.F.S.F. de Moura and J.J.M.S. Domingues: Composites Sci. Technol. Vol. 65 (2005), p. 1948.
10. M.F. Kanninen and C.H. Popelar: *Advanced Fracture Mechanics* (Oxford University Press, Oxford 1985).
11. R.D.S.G. Campilho, M.F.S.F. de Moura and J.J.M.S. Domingues: J. Adhes. Sci. Technol. Vol. 21 (2007), p. 855.